Pergamon

Int. J. Heat Mass Transfer. Vol. 37, No. 6, pp. 1005–1012, 1994

0017-9310/94 $6.00 + 0.00

0017-9310(93)E0002-X

Natural convection heat transfer from a vertical plate—II. With gas injection and transverse magnetic field

AKIRA T. TOKUHIRO† and PAUL S. LYKOUDIS

School of Nuclear Engineering, Purdue University, West Lafayette, IN 47907 U.S.A.

(*Received* 30 *October* 1992 *and in final form* 24 *September* 1993)

Abstract—A natural convection heat transfer experiment was conducted in mercury with gas injection in a vertical enclosure heated on one face at constant heat flux and cooled on the opposite face. Nitrogen gas bubbles were injected from a row of hypodermic tubes facing upwards along the bottom of the heated plate. A transverse magnetic field of magnitude $0.07 \leqslant B \leqslant 0.50$ Tesla was imposed perpendicular to the heated surface. The range of the applied heat flux was $370 \leqslant q'' \leqslant 16\,000$ W m^{-2}, corresponding to a modified Boussinesq number range of $10^5 \leqslant Bo_x^* \leqslant 10^9$. The gas injection rate range was $0.9 \leqslant Q_g \leqslant 9.2$ cm^3 s^{-1}. Local heat transfer and void measurements were made with thermocouple and double-conductivity probes. Experimental results showed that for low heat flux rates, a small magnetic field intensity ($B \sim 0.07$ T) significantly reduced the heat transfer coefficient in the presence of gas injection which in the absence of the magnetic field enhanced the heat transfer coefficient two- to three-fold relative to the single-phase result. The decrease was attributed to the suppression of both the laminar convection and the bubble-induced liquid motion. At higher heat fluxes, the decrease in the heat transfer coefficient in the presence of the magnetic field was less significant. Nevertheless, with increasing field intensity the Nusselt number decreased at these higher heat fluxes. An increase in the bubble size and bubble velocity stabilized the continuous decrease in the heat transfer coefficient for field intensities in the range $B \sim 0.25$–0.35 T. At higher field intensities ($B \sim 0.50$ T) temperature profiles indicated a conduction-dominated heat transfer mechanism.

1. INTRODUCTION

THE INJECTION of gas bubbles into liquid metals is of interest in a number of process applications in the metallurgical industry (see ref. [1]). Two-phase liquid metal flow is also of interest in the design of the blanket in proposed tokamak fusion reactors. Here, one of the possible coolants is a mixture of lithium and helium (see refs. [2, 3]).

In the above applications the convective heat transfer, whether forced or natural, is of fundamental interest. In ref. [4], we have investigated the enhancement of natural convection heat transfer from a vertical plate in contact with mercury with the injection of nitrogen gas bubbles. We found that at low heat fluxes, where the flow along the plate was mostly laminar, the gas injection enhanced the heat transfer coefficient two- to three-fold. Similar results of the heat transfer enhancement were found in water by Wachowiak [5] and in both water and ethyl-alcohol by Tamari and Nishikawa [6]. We attributed these results to the bubble-generated turbulence within the thick laminar thermal boundary layer which greatly enhances the heat transfer mechanism. On the other hand, as the heat flux increased and the flow along the plate became mostly turbulent, the enhancement mechanism was diminished. Void measurements with a double conductivity probe revealed that the bubble-generated turbulence had little effect on the thin turbulent thermal boundary layer since most of the bubbles rise outside the thermal boundary layer. Instead, the bubbles suppressed the thermal stratification present in our enclosure at the higher heat flux rates. Further details on stratification and non-magnetic natural convection heat transfer with gas injection are given in refs. [7, 8].

At the Liquid Metal Thermal-hydraulics Laboratory of Purdue University, a number of magneto-fluid-mechanic (MFM) and heat transfer problems have been examined over the years. Papailiou and Lykoudis [9–11] investigated single-phase laminar and turbulent natural convection in the presence of a transverse magnetic field. In these studies, they reported that a small magnetic field intensity, beginning at $B \sim 0.042$ T, suppressed the liquid motion such that the heat transfer was significantly reduced. In fact for turbulent convection, the magnetic field preferentially suppressed the buoyant component of the turbulent motion and at approximately $B \sim 0.085$ T, the flow field was completely laminarized. Another single-phase MFM natural convection experiment conducted by Seki *et al.* [12] reported that the decrease in the heat transfer coefficient was not as significant for a magnetic field parallel to the heated plate as for

† Address of author for correspondence: Paul Scherrer Institute, Würenlingen, CH-5232 Villigen PSI, Switzerland.

NOMENCLATURE

B magnetic field intensity [T]
Bo_x Boussinesq number, $g\beta\Delta Tx^3/\alpha^2$
Bo_x^* modified Boussinesq number, $NuBo$
D_{ch} bubble chord length [10^{-3} m or mm]
g gravitational constant
Gr_x Grashof number, $g\beta\Delta Tx^3/\nu^2$
Gr_x^* modified Grashof number, $NuGr$
H characteristic heated length [10^{-2} m or cm]
k thermal conductivity [W m^{-1} K^{-1}]
Ly_H Lykoudis number over the length H, $(\sigma_e B^2/\rho)(H/g\beta\Delta T_w)^{1/2}$
Nu_x local Nusselt number, hx/k
Nu_B, Nu_0 Nusselt numbers with and without a magnetic field
Pr Prandtl number, ν/α
Q gas injection rate identifier, Section 3 and Table 1
Q_g gas injection rate [cm^3 s^{-1} or 10^{-6} m^3 s^{-1}]
q'' heat flux rate [W m^{-2}]
Ra Rayleigh number, $g\beta\Delta Tx^3/\alpha\nu$
T_w, T_∞ wall and bulk temperature [°C]
ΔT wall to bulk temperature difference, $T_w - T_\infty$
V_{bub} bubble rise velocity [m s^{-1}]
W heat flux rate identifier, Section 3 and Table 1
X,Y,Z, x,y,z coordinates.

Greek symbols
α void fraction or thermal diffusivity [m^2 s^{-1}]
β coefficient of thermal expansion [°C^{-1}]
σ_e electrical conductivity of fluid [$(\Omega\ m)^{-1}$].

Subscripts and superscripts
B Nusselt-number with magnetic field
bub bubble
ch chord length
e electrical property
g gas
H indicates a quantity over length H
w wall
x indicates a local quantity along x-axis
0 Nusselt-number without a magnetic field
∞ bulk
$''$ Indicates a quantity given as per unit area
* modified quantity; based on q''.

a field perpendicular (transverse) to the plate. In contrast, the experiments of Fumizawa [13] and Takahashi *et al.* [14] produced increased heat transfer coefficients over a certain range of the magnetic field intensity. In Fumizawa's case, the magnetic field was transverse to the heated wall and the heat transfer enhancement was attributed to an η-shaped temperature profile, the origin of which was not indicated. On the other hand in the experiment of Takahashi *et al.*, the bulk temperature was measured in only one location below the cylindrical pin heater. It is possible in both of these experiments that the results were influenced by three-dimensional effects where the fluid is locally accelerated with respect to the applied magnetic field. In general one expects the effect of the magnetic field to produce suppression of the convective motion and a corresponding decrease in the overall heat transfer coefficient.

Although these and other investigations in both magnetic and non-magnetic single- and two-phase liquid metal flows have been conducted, we have not been able to find any experimental investigation in liquid metal natural convection heat transfer with gas injection in the presence of a magnetic field. We therefore set out to investigate this experimentally.

In the sections to follow, the experimental apparatus and experimental procedure will be briefly described in Section 2. Then the experimental results are presented in Section 3. This is followed by a discussion of results in Section 4 and a conclusion in Section 5.

2. EXPERIMENT

The experimental apparatus was previously described in ref. [4] and a detailed description is given in ref. [8]. A schematic of the experimental apparatus is shown in Fig. 1. The apparatus measures 40 cm in height × 7 cm in width × 20 cm in depth (into the figure). The heated plate is 40 cm × 20 cm. The coordinate axes are as follows. The X- and Y-axes are, respectively, parallel and perpendicular to the heated wall while the Z-axis is into the figure. The lower portion of the cooled wall is tapered in accordance with a previous experiment conducted by Papailiou [9]. In this experiment, Papailiou verified the existence of a similarity solution developed by Lykoudis [15] for magneto-fluid-mechanic natural convection with a magnetic field intensity varying as $X^{-1/4}$. Gas injection was provided by 11 equally-spaced hypodermic tubes at the bottom of the heated wall.

The experimental apparatus is inserted in a 20.3 cm gap between the pole faces of an electromagnet powered by a tandem of DC generators. The apparatus is contained within the uniform magnetic field region of the pole faces which are each 127 cm in height by 30.5 cm in width. The magnetic field is transverse to the heated and cooled walls of the experimental cell. In the present experiment, four field intensities of 0.07, 0.25, 0.35 and 0.50 T were applied.

The experiment was conducted by setting the wall heat flux at a predetermined level and adjusting the cooling rate on the opposite side so that the bulk

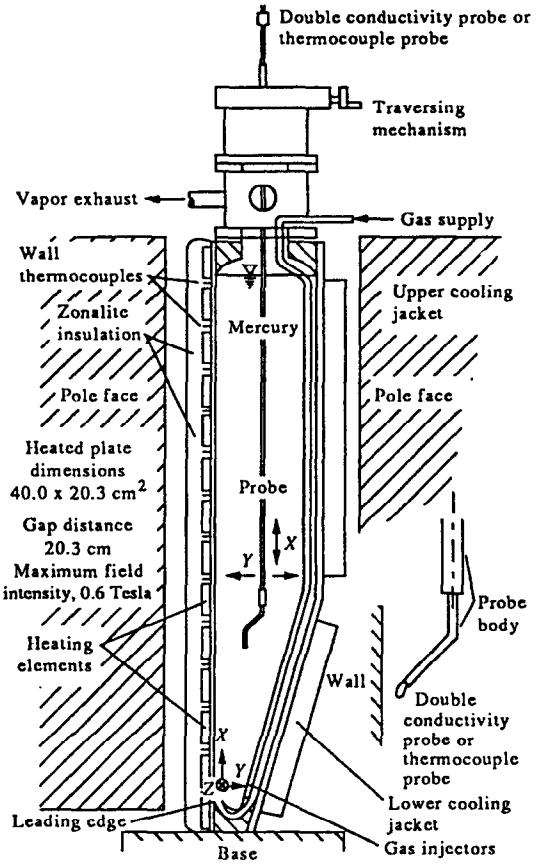

FIG. 1. Schematic of natural convection cell.

temperature could be maintained near room temperature. This was done to minimize heat losses and to maintain a low volumetric concentration of mercury vapor in the laboratory. The bulk temperature was then monitored until a steady state condition was established. Once the bulk temperature ceased to fluctuate by 0.5°C over a 40–60 min period, steady state was assumed to be attained. For laminar convection, this took approximately 6–10 h whereas for turbulent convection, 4–6 h. The magnetic field was then turned on and the bulk temperature was monitored for approximately one hour for the system to again approach steady state conditions. When a steady state condition was reached, the heater voltage, the heater current, the wall temperatures and bulk temperature were recorded. The raw temperature data were than curve-fitted with a polynomial equation using the Sigma-Plot [16] software package. After determining $\Delta T(=T_w-T_\infty)$ and the input heat flux, the local Nusselt and modified Boussinesq numbers were calculated. The thermal properties were evaluated at the average bulk temperature. Further details of the experimental procedures are provided in Tokuhiro [8].

3. RESULTS

The results for both single- and two-phase heat transfer measurements, along with a representative

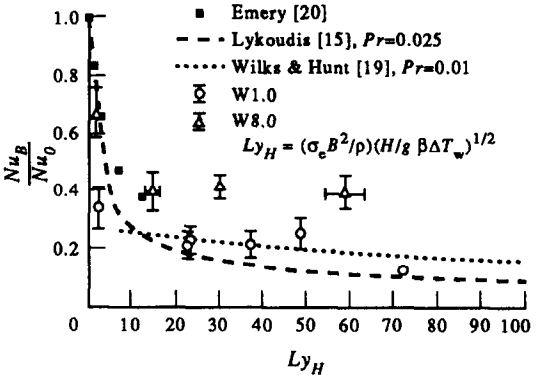

FIG. 2. Ratio of single-phase magnetic to non-magnetic average Nusselt numbers vs the Lykoudis number for heat flux rates W1.0 and W8.0.

set of void measurements, are shown in Figs. 2–7. The void measurements consisted of measurements of the bubble chord length, the bubble rise velocity and the void fraction profile along the Y-axis for a given X-axis location along the heated plate. Representative error bars are indicated in Figs. 2–7. For errors smaller than approximately 10%, the error bars were smaller than the data symbols and are therefore hidden.

In Fig. 2 we show the single-phase natural convection heat transfer result in the presence of a magnetic field. Here, the data are expressed as ratios of the average Nusselt number over the length of the heated plate with a magnetic field to the Nusselt number without a magnetic field ($B = 0$). The Lykoudis number Ly is used to describe the influence of the magnetic field on the natural convection heat transfer.

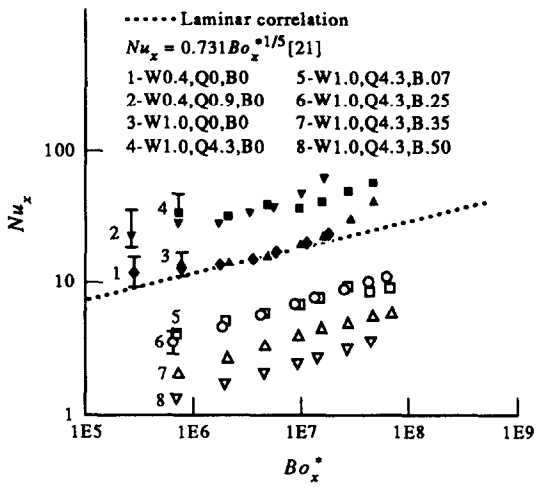

FIG. 3. Local heat transfer data, laminar regime, with gas injection and magnetic field. Where error bars do not appear, the error was less than 10% and hidden behind symbols.

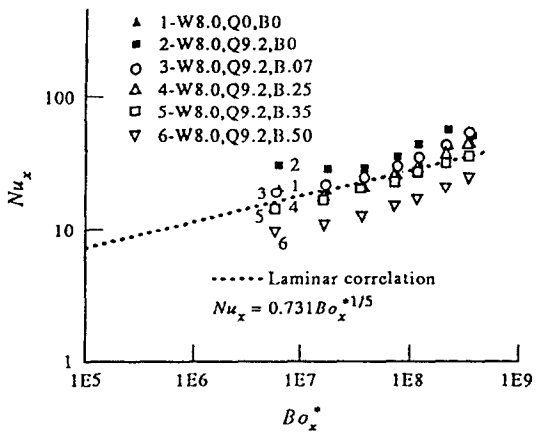

FIG. 4. Local heat transfer data, turbulent regime, with gas injection and magnetic field.

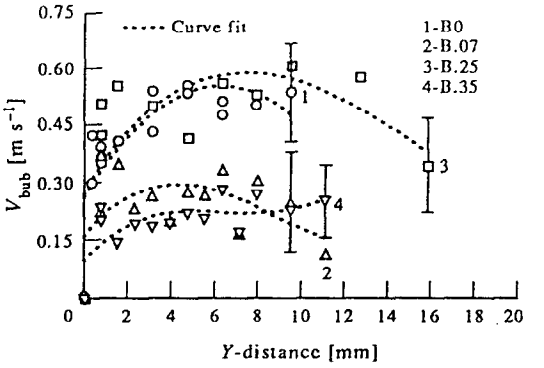

FIG. 6. Bubble rise velocity variation along the Y-axis with gas injection Q4.3, heat flux W1.0 and magnetic field.

This number is defined in ref. [17] as a ratio of the 'free-fall' time to the 'roll-over' time. The 'free-fall' time is the time associated with buoyancy-induced motion in a gravitational field while the 'roll-over' time is the time it takes for a velocity fluctuation in an electrically conducting liquid to be damped by the magnetic field. The Ly number has been traditionally interpreted (see ref. [18]) as the ratio of the ponderomotive force to the square root of the product of the buoyancy and inertial forces. Also shown in the figure are the theoretical solutions of Lykoudis [15] and Wilks and Hunt [19] which begins at an approximate Lykoudis number of $Ly_H \sim 5$. The data points of Emery [20] are also shown in this figure.

It needs to be noted that the theoretical curve in Fig. 2 of Lykoudis [15] is the result of a magnetic field varying with X in the minus one-fourth power, and therefore strictly speaking it would appear not to be relevant to a study with a constant uniform and steady magnetic field. In the experiment of ref. [9] where such a field was created, the lower and higher points along X where such measurements were made were roughly at 15 and 35 cm. To the extent that the Ly number varies with B^2 and hence with the inverse square root of X, the percentage difference from a mean value of Ly was computed to be about $\pm 10\%$. Therefore, the single theoretical curve of ref. [15] in Fig. 2 should be understood to be the mean of two curves plotted with values of $Ly \pm 10\%$. In view of the scatter of the data the relevance of the variable magnetic fields theory with constant magnetic field data, seems to be reasonable.

In Fig. 3 we show the local Nusselt number vs the modified Boussinesq number for the low heat flux rates W0.4 and W1.0. The heat flux rates, gas injection rates and magnetic field intensities were, respectively, coded with the letters W, Q and B followed by a two or three digit number. The corresponding magnitudes are listed in Table 1. In the presence of the magnetic field and gas injection, one low (W1.0) and one high (W8.0) heat flux rate were chosen as representative of natural convection flow which was, respectively, mostly laminar or turbulent along the heated plate. In Fig. 3, the dark symbols show the non-magnetic results in single-phase with gas injection at the two smallest heat flux rates. In both Figs. 3 and 4, a reference line is shown which is the single-phase laminar correlation based on a similarity solution. The laminar correlation was verified to be valid up to $Bo_x^* \sim 5 \times 10^8$

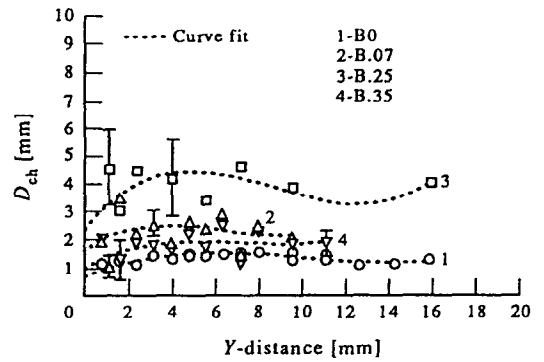

FIG. 5. Bubble chord length variation along the Y-axis with gas injection Q4.3, heat flux W1.0 and magnetic field.

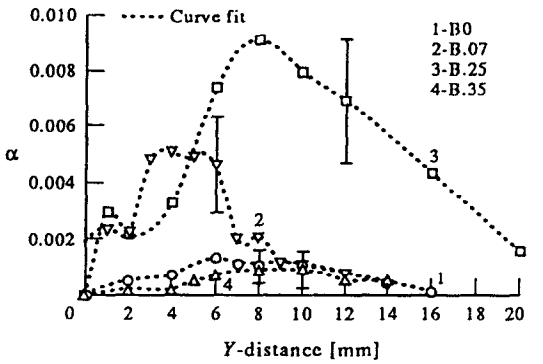

FIG. 7. Void fraction variation along the Y-axis with gas injection Q4.3, heat flux W1.0 and magnetic field.

Table 1. A guide to heat fluxes, gas injections rates and magnetic field intensities

Heat flux rates, kW m^{-2}		
W0.4	represents	$q'' \sim 0.37$
W1.0		$q'' \sim 0.97$
W4.0		$q'' \sim 3.90$
W8.0		$q'' \sim 8.10$
W16.0		$q'' \sim 16.00$
Gas injection rates, cm^3 s^{-1}		
Q0.9	represents	$Q = 0.9$
Q2.1		$Q = 2.1$
Q4.3		$Q = 4.3$
Q9.2		$Q = 9.2$
Magnetic field intensities, T		
B.07	represents	$B = 0.07$
B.25		$B = 0.25$
B.35		$B = 0.35$
B.50		$B = 0.50$
Q0-no injection, B0-no magnetic field		

by Uotani [21]. Figure 3 shows the heat transfer results with gas injection and a magnetic field in open symbols. Figure 4 shows the equivalent data for the higher heat flux rate of W8.0. Here the non-magnetic gas injected case is only shown for the highest gas injection rate, Q9.2. This was chosen since the lower gas injection rates (Q2.1 and Q4.3) showed no enhancement with respect to the single phase result. At the highest injection rate, however, there was a small measure of enhancement. We, therefore, present the magnetic case with the gas injection rate Q9.2.

A representative set of void data which include the bubble chord length, bubble rise velocity and void fraction profile along the Y-axis are, respectively, shown in Figs. 5–7. A polynomial regression line has been drawn through each set of data symbols for visual guidance. These measurements were conducted with a double conductivity probe with an offset distance between the lead probe and the recessed probe of 1.8 mm and a separation distance between them of 2 mm. The measurements were taken at the location $X = 11$ cm. This was a location where a statistically meaningful number of bubbles could be counted.

4. DISCUSSION

4.1. *Single-phase results*

We first discuss the results of single-phase natural convection in the presence of a magnetic field as shown in Fig. 2. Besides our experimental data, the data of Emery [20] are also shown along with the analytical solutions of Lykoudis [15] and Wilks and Hunt [19]. The experiment of Emery was conducted with one wall of an enclosure similar to our apparatus held at constant temperature and for magnetic field intensities in increments of 0.05 T up to 0.2 T.

Figure 2 shows good agreement of Emery's data with the analytical solution of Lykoudis up to $Ly_H \sim 10$ where Emery's points begin to deviate away from the theoretical solution. Unfortunately, an explanation for this trend has not been given. As for the analytical solutions, Lykoudis presented a similarity solution which exists for a magnetic field varying as $X^{-1/4}$ along a semi-infinite plate held at constant temperature. On the other hand, Wilks and Hunt presented a solution which was a synthesis of perturbation and numerical analysis. Their solution did not appear to extend to zero magnetic field but began at approximately $Ly_H \sim 5$. That is, we did not find in their paper a statement that the $B = 0$ case was done nor do we have any reason to suspect that this was not the case.

The agreement between the theoretical solutions and the data is generally good at the lower heat flux rate W1.0. At the higher heat flux rate, W8.0, the experimental data are much higher than the theoretical predictions. The explanation for this disagreement could be sought in three-dimensional effects at higher Ly-numbers. It is well known that in finite enclosures there are regions of secondary motion. It is conceivable that these regions are enhanced in the neighborhood where the induced currents turn around to become parallel to the magnetic field along the enclosure's four corners. In such a case the ponderomotive forces are zero and the local heat transfer remains unaffected by the presence of the magnetic field. Only three-dimensional local measurements could confirm the validity of this speculation.

4.2. *Magnetic results with gas injection*

In the presence of both gas injection and a magnetic field, heat transfer measurements revealed the results presented in Figs. 3 and 4. It is important to note here that, even in the presence of bubbles, mercury is the sole electrically conducting medium interacting with the magnetic field. In addition, the liquid motion is generated not only by the thermal convection but also by the bubbles rising through the fluid.

We first discuss the data at heat flux W1.0, where the thermal boundary layer is predominantly laminar and thick. Here as noted in ref. [4], in the non-magnetic case the bubbles swim inside the thermal boundary layer and generate turbulence along their paths. When small magnetic fields were applied ($B \sim 0.07$ and 0.25 T), the local Nusselt number dropped more than six-fold in comparison to the non-magnetic, gas injected case (W1.0, Q4.3, B0). We attributed this dramatic decrease to the suppression of both the thermally-induced and bubble-induced liquid motion by the ponderomotive force. Similar behavior was observed by Papailiou and Lykoudis [9] in single-phase laminar convection where beginning at $B \sim 0.042$ T, temperature profiles indicated the increasing influence of conduction heat transfer. Additionally in two-phase (bubbly) forced convection flow Gherson and Lykoudis [22] noted a significant

drop in the turbulent intensity for a magnetic field intensity of $B \sim 0.25$ T from hot-film anemometry measurements. As the field intensity increased to $B \sim 0.35$ and 0.50 T we observed a continuing decrease in the Nusselt number. Temperature profile measurements at these field intensities reported by Tokuhiro [8] revealed an increasing linearity in the profile characteristic of conduction-dominated heat transfer. Although not shown here, these profiles were similar to those measured by Papailiou [23].

At the higher heat flux rate, W8.0, the flow along the plate was predominantly turbulent and most of the bubbles rose outside a thin thermal boundary layer as discussed in ref. [4]. With the application of the magnetic field, the local Nusselt number hardly decreased for $B \sim 0.07$ T as shown in Fig. 4 (blank circles). We attributed this behavior to the incomplete suppression of both the thermally and bubble-induced turbulence at this field intensity. Papailiou and Lykoudis [11] found that for turbulent single-phase natural convection, the turbulent fluctuations were completely suppressed and the flow was laminarized for a field intensity of $B \sim 0.085$ T. The Nusselt number decreased further at $B \sim 0.25$ T but remained relatively constant at $B \sim 0.35$ T. This trend was attributed to the change in the bubble size and bubble rise velocity for these field intensities as indicated by void measurements. These trends are discussed in the following section. Further increase of the field intensity to $B \sim 0.50$ T decreased the Nusselt number threefold with respect to the non-magnetic enhanced value (Q9.2, B0). Temperature measurements here revealed a linear profile characteristic of conduction-dominated heat transfer.

4.3. *Void measurements*

The result of the void measurements shown in Figs. 5–7 of the bubble chord length, bubble rise velocity, and void profile aided our understanding of the heat transfer results. The figures included here are representative of similar trends measured at the higher heat flux rate of W8.0. We first consider the change in D_{ch} and V_{bub} along the Y-axis. Figures 5 and 6 indicate that D_{ch} and V_{bub} remain approximately constant at most magnetic field intensities within the scatter of the experimental data but not in all cases. The representative error bar is relatively large due to the wide distribution of bubble sizes ($D_{ch} \sim 1$–10 mm) and the small number of bubble events (detected by the double conductivity probe) especially at larger Y-distances. Given these constraints, a compromise was made in selecting the lead tip to recessed tip distance on the double-conductivity probe. In addition, we note that the void profile as shown in Fig. 7 is not normalized because the probe was not traversed along the Z-axis in order to compute spatially and time-averaged void fractions. Therefore, beyond the recognition that the bubble boundary layer structure consists of three layers, detailed information could not be extracted from the void profiles. The layers

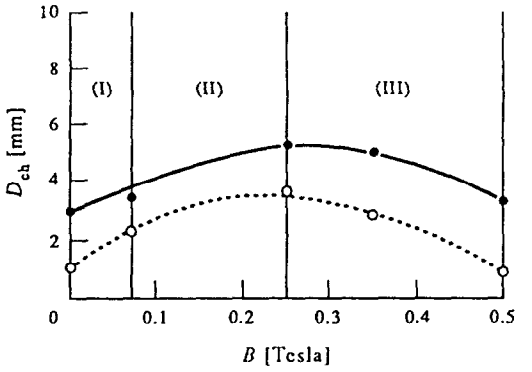

FIG. 8. Qualitative plot of the bubble chord length variation with magnetic field intensity at low and high heat flux rates W1.0 and W8.0.

themselves are the inner single-phase layer next to the heated wall, the middle layer in which most of the bubbles rise and the outer single-phase layer. Further details on the void measurement method are given in Tokuhiro [8]. At this point, in order to facilitate the discussion, we present qualitative graphs of D_{ch} and V_{bub} in Figs. 8 and 9, respectively, as functions of the magnetic field intensity. We do this by taking the average of the maximum and minimum values shown in the corresponding graphs in Figs. 5 and 6. Additionally, in Fig. 10, we present the mean Nusselt number as a function of B taken from Figs. 3 and 4.

We continue our discussion of D_{ch} and V_{bub} through Fig. 10. We first note three regions in Figs. 8 and 9 based on varying trends. Region I marks the initial application of the magnetic field. Here the bubbles remain relatively small and of constant chord length. The bubble velocity, in contrast, decreases due to the immediate suppression of the liquid motion by the ponderomotive force. Here, as in single-phase natural convection, the suppression of the liquid motion is reflected in the Nusselt number which decreases for

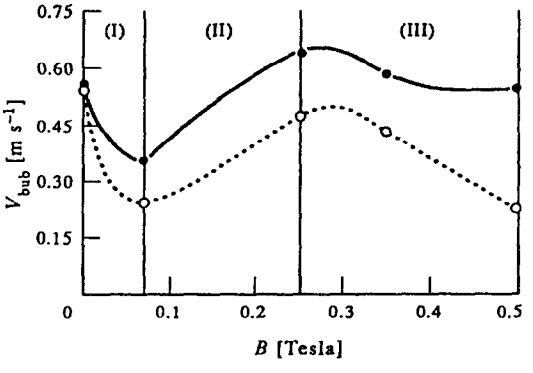

FIG. 9. Qualitative plot of the bubble rise velocity variation with magnetic field intensity at low and high heat flux rates W1.0 and W8.0.

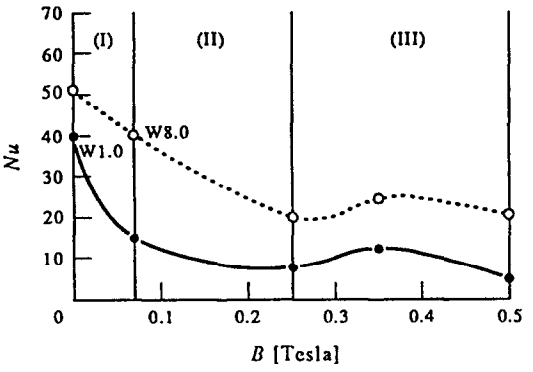

FIG. 10. Qualitative plot of the mean Nusselt number variation with magnetic field at low and high heat flux rates W1.0 and W8.0.

small field intensities. However, at the high heat flux (W8.0) the initial decrease is smaller since there is both thermally- and bubble-induced turbulence prior to the application of the magnetic field. In addition, the suppression of liquid motion thickens the thermal boundary layer and some of the bubbles which were outside the thin turbulent thermal boundary layer in the non-magnetic case now rise through it. This supplies the thermal boundary layer with additional bubble-induced turbulence. As we proceed to region II, the bubbles' chord length increases as well as their rise velocity. Here, the presence of larger bubbles contributes to bubble-generated turbulence making the effectiveness of the ponderomotive force less forceful. As we proceed to region III, the chord length and bubble rise velocity reach a maximum value. Beyond this point, we observe the breakup of bubbles because, presumably, the surface tension cannot sustain them. The breakup of bubbles was also observed and discussed by Gherson and Lykoudis [22] at a magnetic field intensity of $B \sim 0.3$ T. In their forced convection case they reported that the bubble breakup increased the turbulence intensity. Such an increase would contribute to an increase in the heat transfer coefficient. In the present case, temperature profile measurements indicated that the heat transfer was already conduction-dominated. Hence, the breakup had no influence on the heat transfer coefficient.

5. CONCLUSIONS

An experimental investigation of laminar and turbulent natural convection heat transfer from a vertical plate in mercury with gas injection and the presence of a magnetic field was undertaken. The experiment was conducted with the plate held at constant heat flux. Gas was injected to form bubbles from hypodermic tubing at the bottom of the heated section. A uniform transverse magnetic field was imposed on the experimental apparatus. Local heat transfer and void measurements (bubble chord length, bubble rise velocity and void fraction) were taken with the thermocouple and double-conductivity probes.

The heat transfer measurements indicated that in general, the magnetic field decreases the local Nusselt number as a direct consequence of the suppression of the liquid motion by the ponderomotive force. The initial decrease at small magnetic field intensities was more significant in the low heat flux case where the flow was laminar than in the case when the flow was mostly turbulent. The difference was attributed to the presence of both thermally-induced and bubble-induced turbulence at the higher heat flux rate whereas only bubble-induced turbulence was present at the lower heat flux rate. For increasing magnetic field intensities, the local Nusselt number continued to decrease although for the field intensity range, $B \sim 0.25$–0.35 T, the decrease was stabilized. We subsequently found that in this range, both the bubble chord length and bubble rise velocity increased and by giving rise to bubble-induced turbulence, diminished the effectiveness of the ponderomotive force. Beyond $B \sim 0.35$ T there was an indication of bubble break-up and temperature measurements revealed a linearity in the profile (along the Y-axis) characteristic of conduction-dominated heat transfer even in the presence of gas bubbles.

In conducting the experiment we recognized that the bubble parameters are difficult to precisely determine using one double-conductivity probe. It is, therefore, recommended that, in order to further elucidate the influence of bubble dynamics on the heat transfer process, a multiple number of probes be used.

Acknowledgements—The authors would like to express their appreciation to the National Science Foundation who partially supported the research under Grant No. 8304743.

REFERENCES

1. A. Felski, S. N. Waldron and C. Moore. In *Gas Injection into Liquid Metals* (Edited by A. E. Wraith), pp. A.2–A.25. Inst. Min. Metal. and Metal Soc., Univ. Newcastle upon Tyne (1979).
2. M. A. Abdou, M. S. Tillack and A. R. Raffray, Thermal, fluid flow, and tritium release problems in fusion blankets, *Fusion Technol.* **18,** 165–200 (1990).
3. A. Oikawa, T. Kitsunezaki, T. Shibasaki *et al.*, Japanese fusion research: activities in fusion nuclear technology, *Fusion Technol.* **17**(2), 229–315 (1990).
4. A. Tokuhiro and P. S. Lykoudis, Natural convection over a vertical heated flat plate with gas injection and in the presence of a magnetic field, *6th Beer-Sheva Int. Sem. on MHD Flows and Turbulence*, Beer-Sheva, Israel (1990).
5. R. M. Wachowiak, The enhancement of natural convection by rising bubbles, M.S. Thesis, Purdue University, West Lafayette, IN (1986).
6. M. Tamari and K. Nishikawa, The stirring effects of bubbles upon the heat transfer to liquids, *Jap. Res.—Heat Transfer* **5**(2), 31–43 (1976).
7. A. Tokuhiro and P. S. Lykoudis, Natural convection heat transfer from a vertical plate in the presence of stratification, *14th Liquid Metal Boiling Working Group Meeting*, Vol. 2, pp. 491–507. ENEA-Brasimone (1991).

8. A. Tokuhiro, Natural convection heat transfer enhancement in mercury with gas injection and in the presence of a transverse magnetic field, Ph.D. Thesis, Purdue University, West Lafayette, IN (1991).
9. D. D. Papailiou and P. S. Lykoudis, Magneto-fluid-mechanic laminar natural convection—An experiment, *Int. J. Heat Mass Transfer* **11,** 1385–1391 (1968).
10. D. D. Papailiou and P. S. Lykoudis, Turbulent free convection flow, *Int. J. Heat Mass Transfer* **17,** 161–172 (1974).
11. D. D. Papailiou and P. S. Lykoudis, Magneto-fluid-mechanic free convection turbulent flow, *Int. J. Heat Mass Transfer* **17,** 1181–1189 (1974).
12. M. Seki, H. Kawamura, and K. Sanokawa, Natural convection of mercury in a magnetic field parallel to the gravity, *Trans. ASME, J. Heat Transfer* **101,** 227–232 (1979).
13. M. Fumizawa, Natural convection experiment with liquid NaK under transverse magnetic field, *J. Nucl. Sci. Technol.* **17**(2), 98–105 (1980).
14. O. Takahashi, N. Nagase, I. Michiyoshi and N. Takenaka, Natural convection heat transfer from a vertical cylindrical heat to liquid metals under horizontal magnetic field, *8th Int. Heat Transfer Conf.*, Vol. 2, pp. 1317–1322. Hemisphere, New York (1986).
15. P. S. Lykoudis, Natural convection of an electrically conducting fluid in the presence of a magnetic field, *Int. J. Heat Mass Transfer* **5,** 23–34 (1962).
16. Sigma-Plot (Trademark), Version 3.1, Jandel Scientific, Sausalito, CA (copyright 1987).
17. P. S. Lykoudis, Non-dimensional numbers as ratios of characteristic times, *Int. J. Heat Mass Transfer* **33,** 1568–1570 (1990).
18. Dimensionless Groups. In *CRC Handbook of Chemistry and Physics* (Edited by R. C. Weast) (52nd Edn.), p. F-273. The Chemical Rubber Co., Cleveland, U.S.A. (1971–72).
19. G. Wilks and R. Hunt, Magnetohydrodynamic free convection about a semi-infinite plate whose surface the heat flux is uniform, *J. Appl. Math. Phys.* **35,** 34–49 (1984).
20. A. F. Emery, The effect of a magnetic field upon the free convection of a conducting fluid, *Trans. ASME, J. Heat Transfer*, 119–124, May (1963).
21. M. Uotani, Natural convection heat transfer in thermally stratified liquid metal, *J. Nucl. Sci. Technol.* **24**(6), 442–451 (1987).
22. P. Gherson and P. S. Lykoudis, Local measurements in two-phase liquid-metal magneto-fluid-mechanic flow, *J. Fluid Mech.* **147,** 81–104 (1984).
23. D. D. Papailiou, Magneto-fluid-mechanic tubulent free convection, Part I, Ph.D. Thesis, Purdue University, West Lafayette, IN (1971).